



OPEN ACCESS

EDITED BY
Carlos M. Costa,
University of Minho, Portugal

REVIEWED BY
Umapathi Reddicherla,
Inha University, South Korea
Sheng Chen,
Xiangtan University, China

*CORRESPONDENCE
H. B. Duan,
duanhaibao4660@163.com

†These authors have contributed equally
to this work

SPECIALTY SECTION
This article was submitted to
Piezoelectric Materials,
a section of the journal
Frontiers in Electronic Materials

RECEIVED 27 July 2022
ACCEPTED 31 August 2022
PUBLISHED 21 September 2022

CITATION
Yu SS, Zhao HR, Xu W, Zhang H and
Duan HB (2022), Switchable magnetic,
dielectric, conductivity, and phase
transition properties of charge-
transfer crystals.
Front. Electron. Mater. 2:977164.
doi: 10.3389/femat.2022.977164

COPYRIGHT
© 2022 Yu, Zhao, Xu, Zhang and Duan.
This is an open-access article
distributed under the terms of the
[Creative Commons Attribution License
\(CC BY\)](https://creativecommons.org/licenses/by/4.0/). The use, distribution or
reproduction in other forums is
permitted, provided the original
author(s) and the copyright owner(s) are
credited and that the original
publication in this journal is cited, in
accordance with accepted academic
practice. No use, distribution or
reproduction is permitted which does
not comply with these terms.

Switchable magnetic, dielectric, conductivity, and phase transition properties of charge-transfer crystals

S. S. Yu^{1†}, H. R. Zhao^{1†}, W. Xu², H. Zhang¹ and H. B. Duan^{1,2*}

¹School of Environmental Science, Nanjing Xiaozhuang University, Nanjing, China, ²Department of Chemistry, Huangshan University, Huangshan, China

The properties can be switched between different states and can be used in sensors, displays, and memory devices. In this study, two multi-functional switchable materials [C₅-Pmim][Ni(mnt)₂] (1) and [C₆-Hmim][Ni(mnt)₂] (2) (where mnt²⁻ = maleonitriledithiolate, C₅-Pmim = 1-pentyl-3-methylimidazolium, and C₆-Hmim = 1-hexyl-3-methylimidazolium) have been designed and synthesized, which has segregated cation and anion stacks in the crystal structure. 1 shows two-step switchable dielectric transition with a thermal hysteresis loop accompanying structure phase transition. Dielectric transition of 1 can be attributed to the reorientation of the polar cations and crystal to mesophase transition. Switchable conductivity properties of 1 and 2 were realized by the crystal to mesophase structure transition. The conductivity of the mesophase for 1 and 2 is higher than the corresponding crystal phase. Furthermore, magnetic phase transition with the non-common hysteresis loop for 2 is observed being triggered by the structure and dielectric transition. To the best of our knowledge, this study might be the rare multi-functional switchable examples with dielectric, conductivity, and magnetic transition.

KEYWORDS

Bis(maleonitriledithiolato)nickelate monoanion, switchable dielectric, magnetic transition, conductivity, phase transition

Introduction

Systems that can change their physical or chemical properties by external stimuli, such as temperature, light, pressure, and electric or magnetic fields, and some special chemical materials are interesting. The properties can be switched between different states and can be used in sensors, switches, memory devices, and so on (Delaire and Nakatani, 2000; Yu et al., 2003; Samoc et al., 2006; Stuart et al., 2010). Spin-crossover (SCO) compounds are the most interesting examples of the switchable magnetic state, which possess labile electronic configurations and different dielectric constant, magnetic, and optical properties in the high-spin and low-spin state (Weber et al., 2008; Weber, 2009; Lochenie et al., 2014; Matsumoto et al., 2014). On the other hand, the one-dimensional (1D) S = ½ Heisenberg spin chain compound is also a cooperative

electronic system with switchable spin-Peierls transition properties. In previous studies, we have designed and achieved a series of one-dimensional (1D) spin-Peierls-type transition compounds (Duan et al., 2011; Duan et al., 2013; Yu et al., 2013), which show a paramagnetic-to-nonmagnetic switchable phase transition.

Analogous to the switchable magnetic state compounds, switchable dielectrics with the high–low dielectric state in response to temperature and applied electric field have attracted a great deal of attention for their widespread applications in photonic devices, optoelectronic technology, and digital processing, etc (Xu et al., 2010; Salinga and Wuttig, 2011; Champagne et al., 2012; Sun et al., 2012). The dielectric constant $\epsilon^* = \epsilon' - i\epsilon''$ can reflect the molecular motion and reorientational motion of polar molecules or ions in crystals. From a microscopic point of view, the dynamic motion of a moiety in a molecular system, such as order–disorder transformation, reorientation, and rotational motion, plays a crucial role in the design of switchable dielectric materials (Fu et al., 2013; Sun et al., 2014; Asghar et al., 2016). Garcia-Garibay group-designed amphidynamic crystals contain rigid and mobile parts within the same molecule, which is a feasible approach to the design of switchable dielectric materials because mobile parts can reorient and respond to the external electric field. Akutagawa et al. (2009) obtained flip-flop supramolecular rotators with switchable dielectric properties by using rotary molecule motion. Some one-dimensional perovskite compounds using organic ammonia cations as rotating parts may be a good candidate for switchable dielectric materials (Hang et al., 2011). Recently, our group reported hydrogen-bonded diazabicyclo [2.2.2]octane molecular rotors that showed high–low dielectric state transition in response to the external electric field and temperature (Jiang et al., 2019). The methylimidazolium cation is a representative cation of ionic liquids, which consist of a heterocyclic aromatic ring with two different alkyl chains attached. It has been shown that the unique thermodynamic properties of methylimidazolium are mainly induced by the cooperative rotation motion of the alkyl chain (Hamaguchi and Ozawa, 2005). Similar behavior is often observed in ionic liquids (Su et al., 2015).

With the aforementioned findings in mind, we turned our focus on alkyl derivatives—the potential rotors. In this study, methylimidazolium was chosen as cations and reacted with the $[\text{Ni}(\text{mnt})_2]^-$ (mnt^{2-} = maleonitriledithiolate) spin system, with the aim of creating multi-functional bistability materials. This objective has been achieved through the preparation of the compounds $[\text{C}_5\text{-Pmim}][\text{Ni}(\text{mnt})_2]$ (1) and $[\text{C}_6\text{-Hmim}][\text{Ni}(\text{mnt})_2]$ (2) ($\text{C}_5\text{-Pmim}$ = 1-pentyl-3-methylimidazolium; $\text{C}_6\text{-Hmim}$ = 1-hexyl-3-methylimidazolium). 1 and 2 exhibit remarkable dielectric phase transition with switching characteristics and is relevant to cooperative rotation motion of the alkyl chain and structure phase transition. Furthermore, 2 shows magnetic transition with the non-common shape of the

hysteresis loop in the heating/cooling processes induced by structure phase transition. The phenomenon of a magnetic transition has, in general, been observed in the $[\text{Ni}(\text{mnt})_2]^-$ spin systems whilst is very uncommon with magnetic, dielectric, and conductivity transition in such systems.

Experimental section

Na_2mnt was synthesized by the method described in the literature (Davison and Holm, 1967), and $[\text{C}_5\text{-Pmim}]\text{Br}$, $[\text{C}_6\text{-Hmim}]\text{Br}$, $[\text{C}_5\text{-Pmim}]_2[\text{Ni}(\text{mnt})_2]$, and $[\text{C}_6\text{-Hmim}]_2[\text{Ni}(\text{mnt})_2]$ were prepared employing the similar procedure of the literature (Tian et al., 2009).

Preparation of $[\text{C}_5\text{-Pmim}][\text{Ni}(\text{mnt})_2]$

1) MeOH solution (10 cm³) of I_2 (205 mg, 0.80 mmol) was slowly added to MeOH solution (25 cm³) of $[\text{C}_5\text{-Pmim}]_2[\text{Ni}(\text{mnt})_2]$ (1.0 mmol); after stirred for 25 min, the mixture was allowed to stand overnight. The microcrystalline precipitate formed was filtered off, washed with MeOH, and dried in vacuum.

A similar procedure was used for the preparation of 2, and the final product of each compound was dried at 80°C under vacuum for microanalysis.

The single crystals of 1 and 2, suitable for single-crystal x-ray diffraction, were obtained by slow evaporation of the corresponding compounds in methanol at an ambient temperature.

Physical measurements

Magnetic susceptibility data of polycrystalline samples of 1 and 2 were collected over the temperature range of 2–400 K using a Quantum Design MPMS-5 superconducting quantum interference device (SQUID) magnetometer, and the diamagnetic correction was performed utilizing Pascal's constants. TGA and DTA experiments were performed using a TA 2000/2960 thermogravimetric analyzer at the temperature ranging from 20 to 800°C for 1 and 2 at a warming rate of 10°C/min under a nitrogen atmosphere, and the polycrystalline samples were placed in an aluminum crucible. DSC experiments were carried out on a Pyris 1 power-compensation differential scanning calorimeter in the temperature range of -50–130°C at a warming and cooling rate of 10°C/min under a nitrogen atmosphere for 1 and 2. Powder X-ray diffraction (PXRD) measurements were performed on a Bruker D8 diffractometer with Cu-K α radiation ($\lambda = 1.5418 \text{ \AA}$). Temperature- and frequency-dependent dielectric spectra were carried out employing a

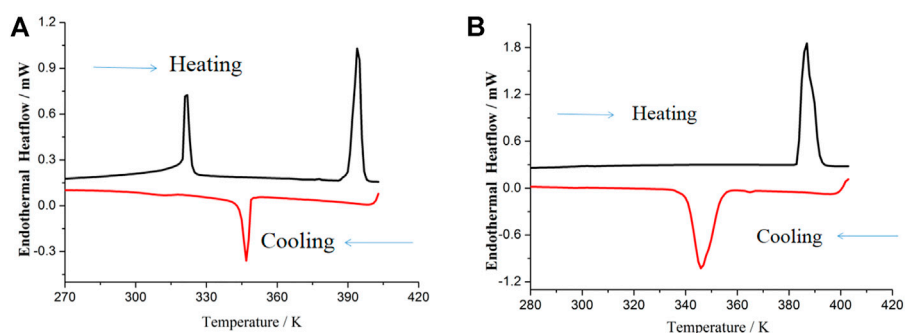


FIGURE 1
DSC plots for (A) 1 and (B) 2 (at a heating/cooling rate of 10 K/min).

Concept 80 system (Novocontrol, Germany) under the N_2 atmosphere in the temperature range of 223–413 K for 1 and 223–393 K for 2 with the heating/cooling cycle.

X-ray single crystallography

Selected crystals were centered on an Oxford Diffraction Xcalibur diffractometer equipped with a Sapphire 3 CCD detector and a mirror monochromated Cu-K α radiation ($\lambda = 1.54184 \text{ \AA}$). The data collection routine, unit cell refinement, and data processing were carried out using the CrysAlis program (CrysAlis, 2004). Structures were solved by the direct method and refined by the SHELXL-97 software package (Sheldrick, 1997). The non-hydrogen atoms were refined anisotropically using the full-matrix least-squares method on F (Weber et al., 2008; Weber, 2009). All H atoms were placed at calculated positions (C-H): 0.930 \AA for pyridine, 0.970 \AA for methylene, and 0.860 \AA for -NH₂ and refined riding on the parent atoms with $U(H) = 1.2U_{eq}$ (bonded C or N atoms).

Results and discussion

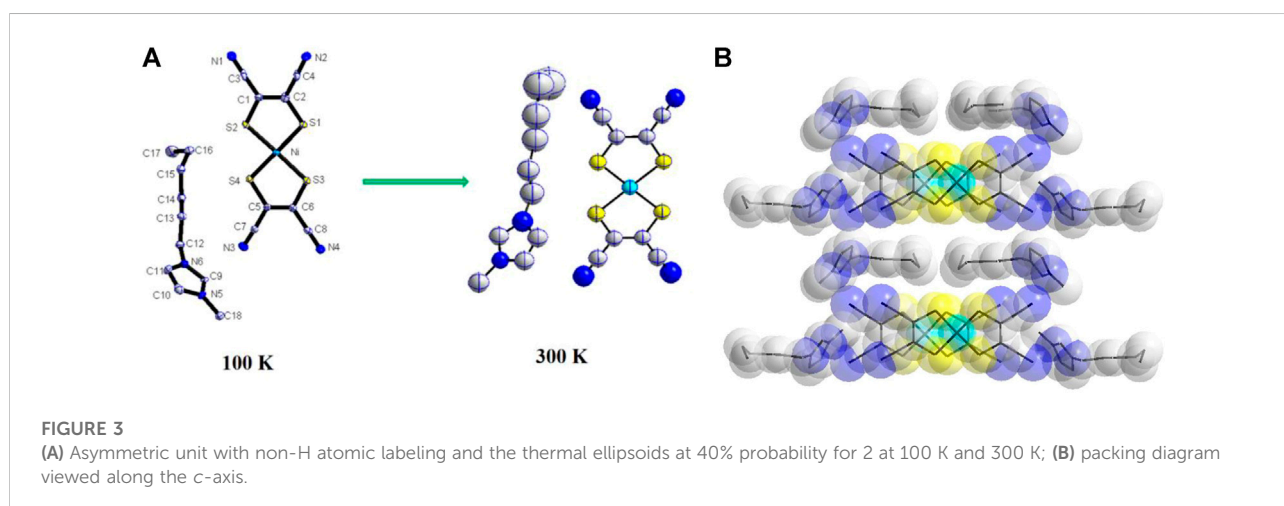
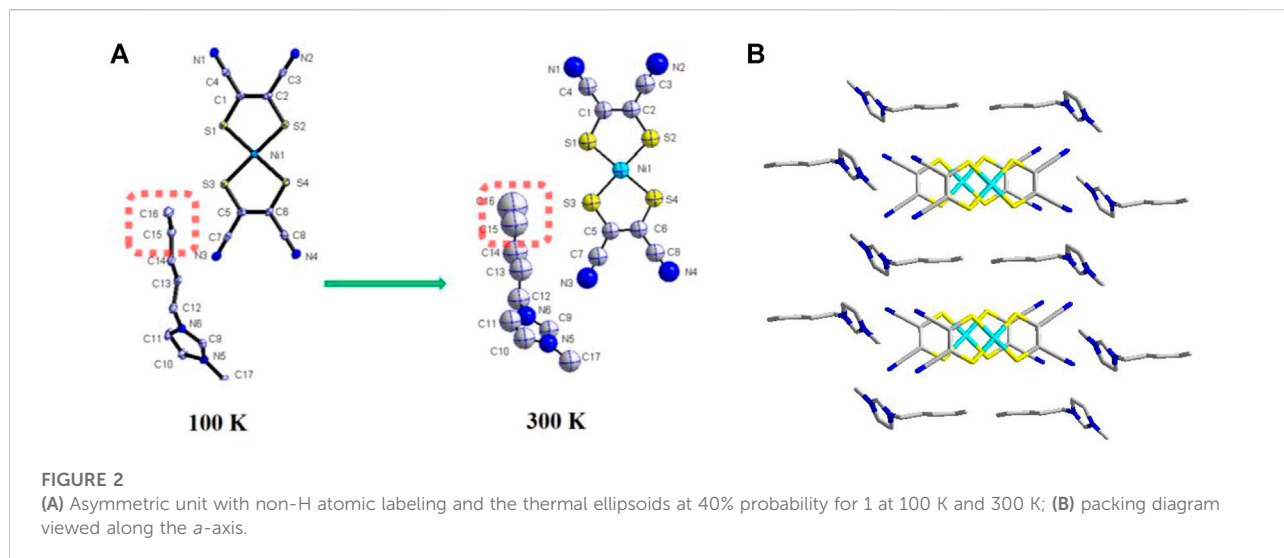
DSC traces of 1 and 2 are shown in Figure 1, from which it can be found that the two compounds showed thermal hysteresis behavior during the heating/cooling cycle. Two endothermic events appear in the plots of DSC traces before melting of 1 (Figure 1A). The first endothermic event approximately at 322 K is assigned to the transition of the crystal phase to crystal phase, and the second endothermic event approximately at 394 K probably corresponds to the transition of the crystal phase to mesophases. The two-step phase transition temperature of 1 is in good agreement with the two-step dielectric relaxation temperature (discussion in the next section). In the following cooling run of 1, only one endothermic event occurred approximately at 346 K, which can be ascribed to the

transition of the mesophase to crystal phase. The thermal hysteresis at about 48 K was observed for 1. As displayed in Figure 1B, 2 shows one endothermic event approximately at 387 K in the heating run, corresponding to the transition of the crystal phase to mesophases, which is in agreement with the dielectric transition results of 2. In the cooling run, the endothermic event for the transition from the mesophase to the crystal phase occurred approximately at 345 K.

Compound 1 crystallizes in a triclinic space group P-1 at 100 K; its asymmetric units are one $[\text{Ni}(\text{mnt})_2]^-$ and one $\text{C}_5\text{-bmim}^+$ (Figure 2A). The most bond lengths and angles in $[\text{Ni}(\text{mnt})_2]^-$ agree well with those in the reported $[\text{Ni}(\text{mnt})_2]^-$ compounds (Tian et al., 2009). The cation adopts a bent conformation, and its hydrocarbon chain shows trans conformation. As displayed in Figure 2B, the anions and cations form segregated stacks along the crystallographic *a*-axis direction. In anions stacks, the adjacent $[\text{Ni}(\text{mnt})_2]^-$ anions formed into a cofacial π -type dimer. Ni-Ni distances are 3.733(6) \AA and 4.237(6) \AA , respectively. The shorter interatomic separations in an anion stack is 3.442(7) \AA of S(3) ... S(4)^{*i*} (symmetric codes *i* = 1-*x*, 1-*y*, 1-*z*). Each anion stack is surrounded by six cation stacks. Along the *c*-axis direction, cations adopt the tail-to-tail model arrangement.

The crystal structure of 1 at 300 K is similar to that at 100 K. The space group is not changed, and the cell parameter is also an analog to that at 100 K. The main change is with the atom thermal displacement parameters. The values of U_{eq} for C(15) and C(16) show a rapid increase as the temperature increases from 100 to 300 K (Figure 2A), which indicates that there exists thermal-activating rapid motion for the alkyl chain of $[\text{C}_5\text{-bmim}]^+$ cation.

Compound 2 crystallizes in a monoclinic space group $P2_1/c$ at 100 K, and the asymmetric units are one $[\text{Ni}(\text{mnt})_2]^-$ and one $\text{C}_6\text{-bmim}^+$ (Figure 3A). The planar $[\text{Ni}(\text{mnt})_2]^-$ anions show similar geometric parameters to 1. Different from 1, the hydrocarbon chain of the counteranion in 2 shows a mixed conformation also, where C(12), C(13), C(14), and C(15) adopt completely trans conformation, and C(15), C(16), and C(17) in the hydrocarbon chain adopt cis conformation. The direction of



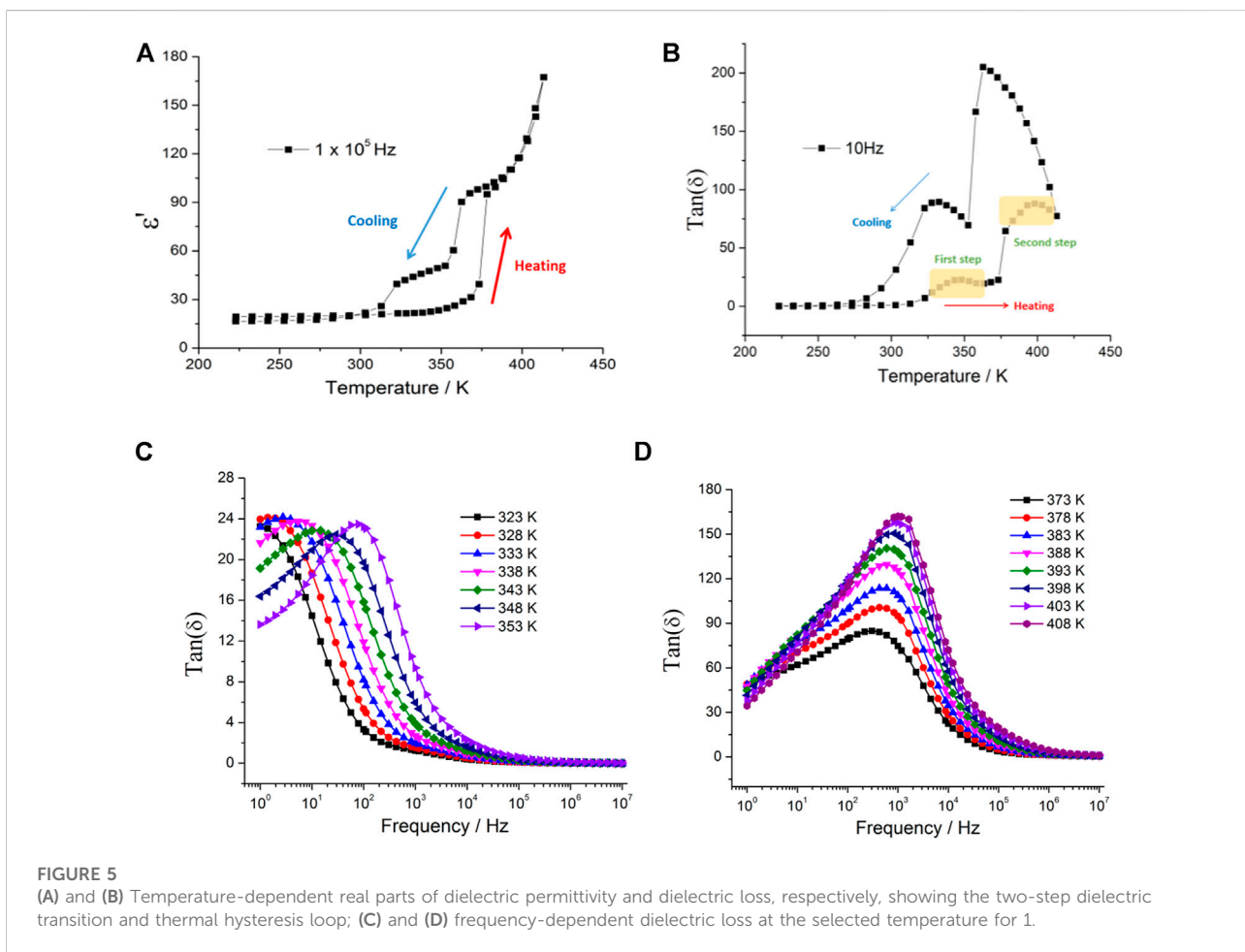
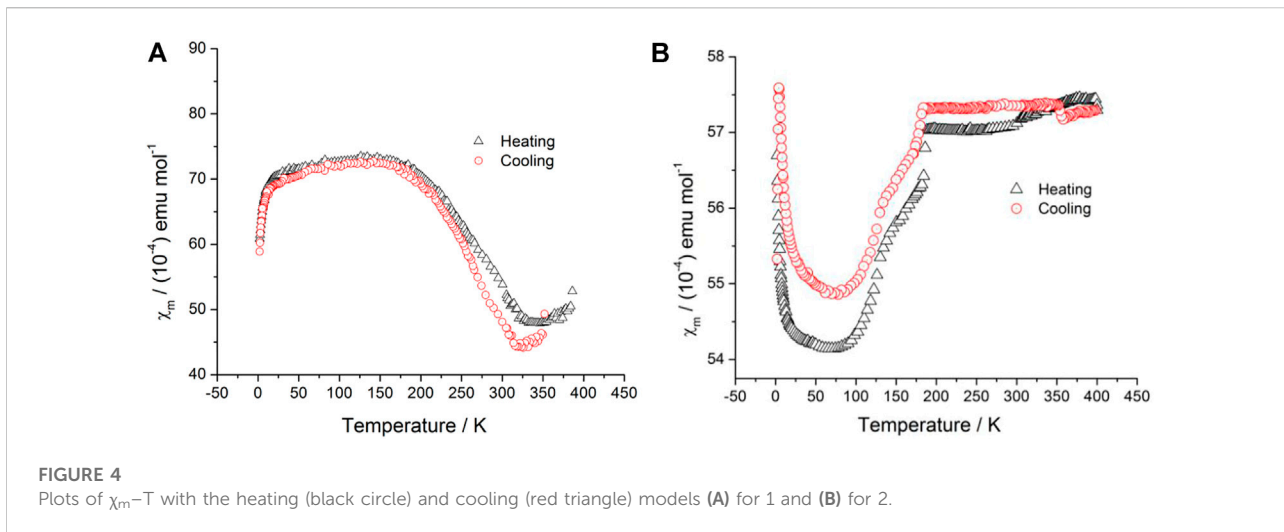
the hydrocarbon chain is approximately parallel to the long molecular axis of the $[\text{Ni}(\text{mnt})_2]^-$ anion in 2. The packing structure of 1 and 2 is very similar, and the anions and cations of 2 also form segregated stacks along the crystallographic *c*-axis direction (Figure 3B). However, the regular anion stacks were observed in 2 with the nearest Ni–Ni distances of 4.099(6) Å.

From 100 to 300 K, the molecule conformation and packing structure of 2 are not changed, and the cell parameters are analogs to those at 100 K. The thermal motion of the $\text{C}_6\text{-bmim}^+$ cation can be reflected in atom thermal displacement parameters. The values of U_{eq} for C(15), C(16), C(17), and C(16) show a rapid increase as the temperature increases from 100 K to 300 K (Figure 3A), which is similar to the situation of 1.

Magnetic susceptibility data of polycrystalline samples of 1 and 2 were collected over the temperature range of 2–400 K,

and the plot of χ_m versus *T* is displayed in Figure 4A and Figure 4B. The magnetic behavior of 1 and 2 is different. For 1, a Curie-type paramagnetism tail was not observed in the low-temperature region (Figure 4A). From 20 to 153 K, the χ_m value did not almost change. When the temperature rose above 200 K, the χ_m value underwent an abnormal rapid decrease and reached a plateau point at 330 K. With the temperature further increased, the χ_m value slightly increased. Interestingly, a thermal hysteresis loop occurred in the heating/cooling cycle.

On the contrary, a rather complicated magnetic behavior was observed for 2 (Figure 4B). In the heating process, the χ_m value dropped abruptly with Curie-type paramagnetism in the low-temperature region (below 50 K). As the temperature rose above 120 K, the χ_m value jump was observed and reached a plateau point at 188 K, suggesting an occurrence of a magnetic transition. From 188 to 400 K, the χ_m value did not almost change. The



shape of χ_m -T plots in the heating process is similar to the cooling process, and it is noticeable that the χ_m -T plot in the cooling process is diverged. Thus, the non-common shape of the

hysteresis loop occurs. Such types of hysteresis loops have also been reported in some spin-crossover mesophase systems and interpreted as due to the supercooling of mesophase (where a

crystalline-to-mesophase transformation and a spin-crossover process occur in the same temperature interval) (Seredyuk et al., 2008). Combined with the DSC results of 1 and 2, the obvious supercooling occurred in 1 and 2, which is relevant to the conformation of the ion liquid cation. Thus, the non-common magnetic transition can be ascribed to the supercooling behavior of 1 and 2.

Supplementary Figure S1 shows the temperature-dependent complex dielectric constant of 1, $\epsilon^* = \epsilon' - j\epsilon''$. Both the real (ϵ') and imaginary (ϵ'') parts of the complex dielectric constant exhibited a two-step marked increase with temperatures above 312 K and 352 K at $f = 10^5$ Hz (Figure 5A), and the dielectric constant was dependent on the frequency of the applied electric field. These features of dielectric responses are characteristics of reorientational motion of polar molecules or ions in crystals. Interestingly, the irregular thermal hysteresis loop was observed in the dielectric constant of 1 from 378 to 300 K in the cooling process (Figure 5A). In general, when the polar molecule reorientation is compared with the frequency of the applied alternating electric field, the dielectric loss occurs as peaks because the phase lag results in the absorption of energy by the materials. As shown in Figure 5B, two dielectric loss peaks were observed corresponding to the two-step dielectric response from 321 to 412 K at $f = 10$ Hz, and the thermal hysteresis loop occurred in the cooling process. With the frequency increased to $f = 10^5$ Hz (Supplementary Figure S2), the dielectric loss peaks almost disappeared, and the value of $\tan(\delta)$ rapidly decreased, which indicated that the dipole molecule motion is too slow to follow the switching of the electric field. From the plots of frequency-dependent dielectric constant (Supplementary Figure S3), the ϵ' value sharply decreased with the increase in frequency. The molecule dipoles are almost stationary and do not contribute to the dielectric constant in the high-frequency region. Figure 5C shows the frequency-dependent dielectric loss, from 323 to 353 K (the first step dielectric response in Figure 5B). The dielectric loss peaks were observed in the low-frequency region and shifted to the high-frequency region with the increase in temperature. The first step dielectric response can be attributed to the reorientation of the polar organic cations, and the $[\text{Ni}(\text{mnt})_2]^-$ anions do not contribute to the orientational polarization. The second dielectric response shows a weak temperature-dependent relationship (Figure 5D), and the position of dielectric loss peaks did not almost change from 373 to 408 K, which may be relevant to the structure phase transition and is consistent with the DSC results. When the temperature increases higher than 373 K, the value of dielectric loss is very high, indicating the rapid increase in the conductivity of the sample.

Supplementary Figure S4 and Figure 6A show the temperature-dependent real part complex dielectric constant of 2. The dielectric constant remains stable at about

11–13 below 350 K, and then it displays a pronounced change to high dielectric states with a step-like anomaly at above 365 K at $f = 10^5$ Hz (Figure 6A). In the following cooling process, the similar dielectric phase transition was observed, and the heating/cooling cycle showed a narrow thermal hysteresis. From the microscopic viewpoint, the tunable dielectric constant may be related to the positional and orientational variation of molecular dipole moments. Combined with the DSC results, the dielectric phase transition of 2 was attributed to structure phase transition. The temperature-dependent dielectric loss also showed a step-like anomaly near to the phase transition temperature (Figure 6B). The frequency-dependent dielectric constant showed dielectric relaxation in the low-frequency region (Figure 6C), and the dielectric constant increased with the increasing temperature, indicating that the thermally activated dipole motion is suppressed in the low-temperature region. In order to reduce the influence of direct current conduction and electrode polarization on the low-frequency region, dielectric modulus was used to analyze dielectric relaxation of 2. The dielectric constant can be transformed into dielectric modulus using the following equation:

$$M^*(\omega) = \frac{1}{\epsilon^*(\omega)} = \frac{\epsilon' + j\epsilon''}{\epsilon'^2 + \epsilon''^2} = M' + jM'',$$

where M' and M'' are the real and imaginary parts of the complex modulus M^* , respectively. The plots of $M''-f$ are shown in Figure 6D for 2. The modulus peak shifts to the high-frequency region with the increase in temperature.

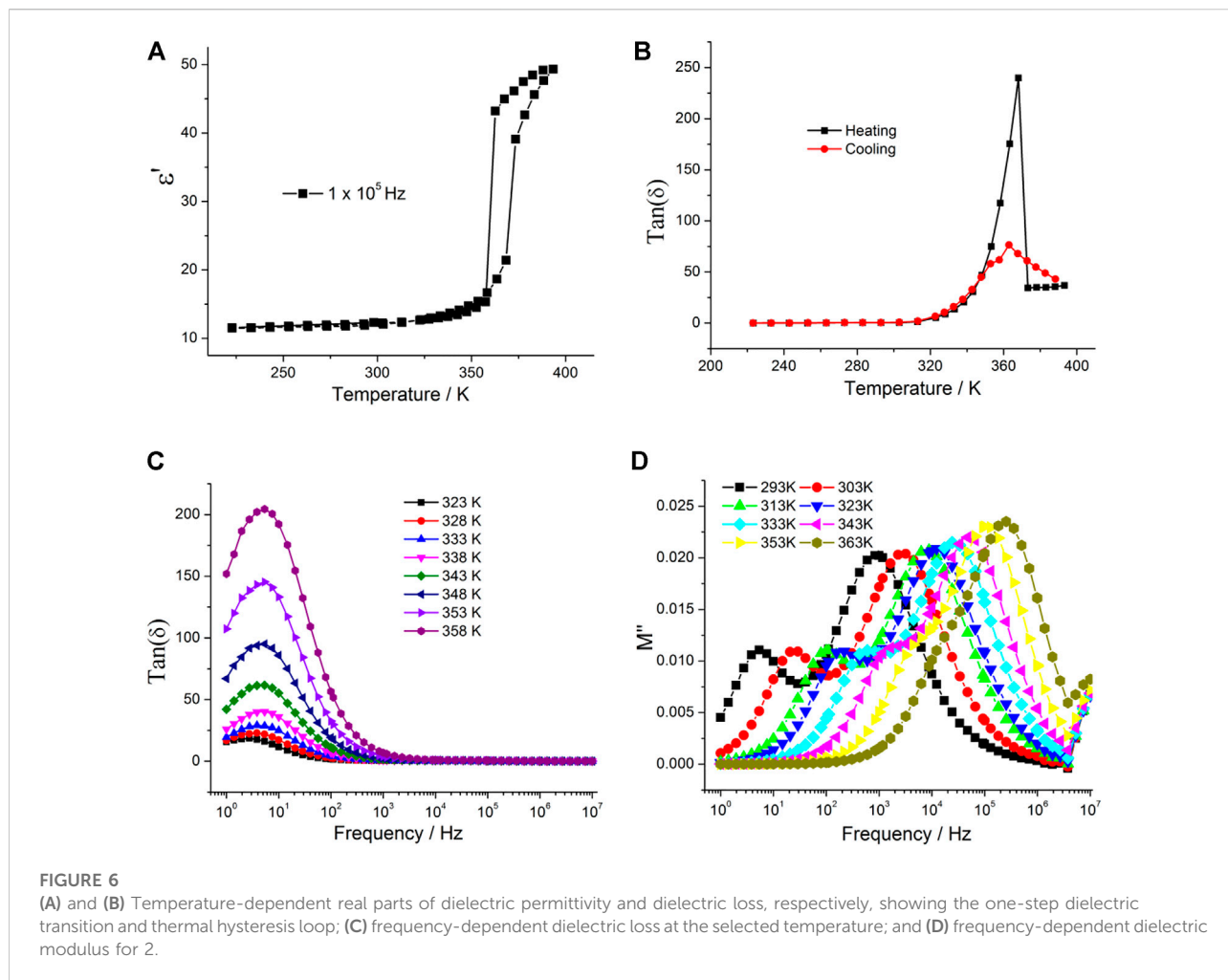
Ionic conductivity

The real $Z(\omega)$ and imaginary $Z(\omega)$ parts of the complex impedance $Z^*(\omega) = Z(\omega) - Z(\omega)$ can be estimated by using the following relations (Mariappan et al., 2005):

$$Z'(\omega) = \frac{G}{G^2 + \omega^2 C^2},$$

$$Z''(\omega) = \frac{C\omega}{G^2 + \omega^2 C^2},$$

where G and C are the measured parallel conductance and the capacitance, respectively. The impedance spectra can be interpreted by means of an equivalent circuit where each impedance semicircle can be represented by resistor, R , and capacitor, C in parallel (parallel RC element) (Barsoukov and Macdonald, 2018). Figure 7A and Supplementary Figure S5 show the impedance plots of 1 in the form of Cole–Cole plots at selected temperatures. A large semicircle at a high frequency and an inclined spike at a low frequency were observed. The semicircle that occurred in the high-frequency region can be attributed to the conductivity of grains, and the spike observed in the low-frequency region can be attributed to the grain boundary and electrode polarization. It can be seen from the



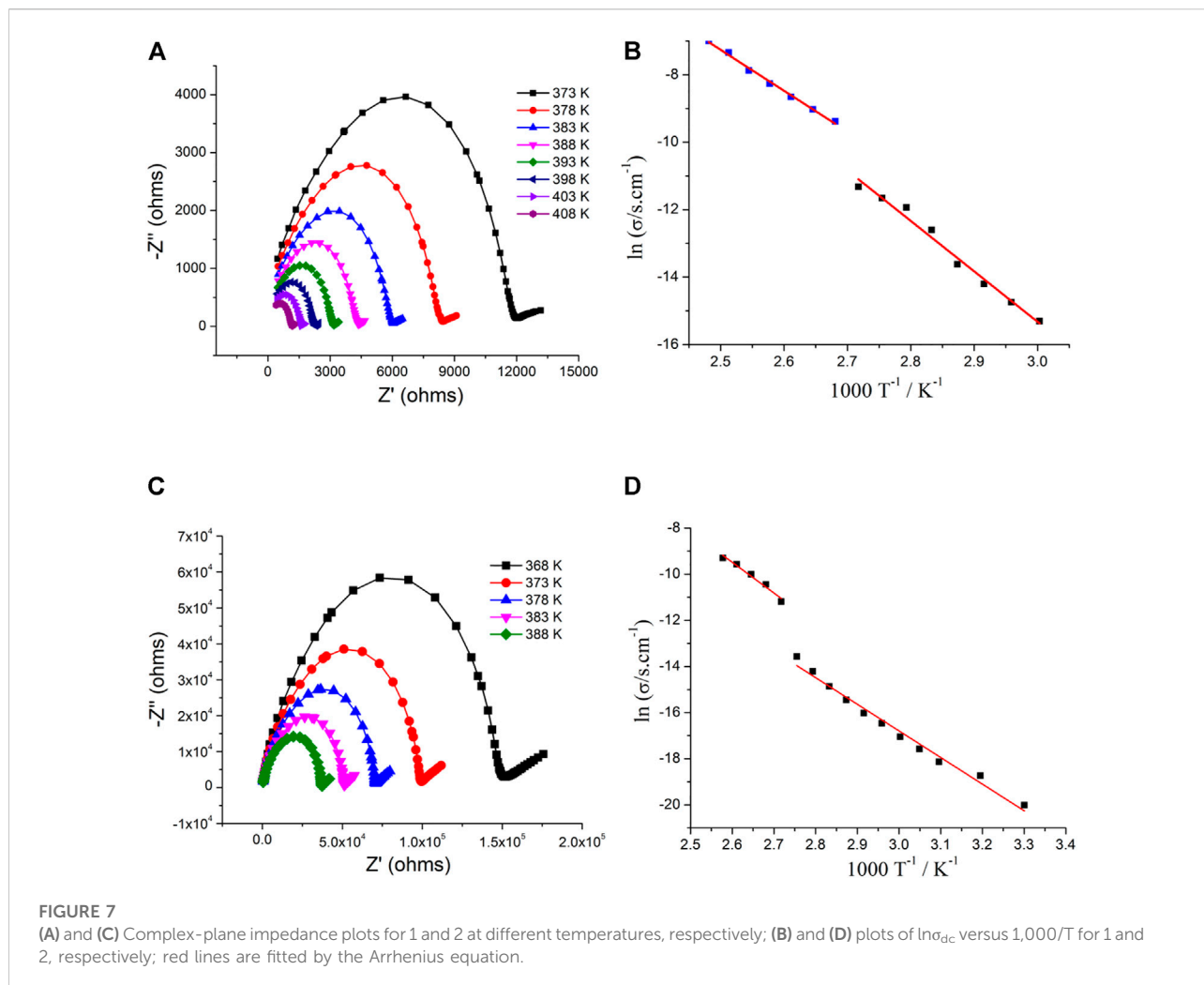
plots that as temperature increases, the radius of the arc decreases, indicating the conductivity increase of 1 (thermally activated conduction phenomena). σ_{dc} can be obtained by fitted impedance data using an equivalent circuit. As shown in Figure 7B, the values of conductivity of 1 is $2.25 \times 10^{-7} \text{ S cm}^{-1}$ at 333 K and $1.21 \times 10^{-5} \text{ S cm}^{-1}$ at 368 K. A steep increase was observed from 368 K to 373 K and reached $8.43 \times 10^{-5} \text{ S cm}^{-1}$. This variation is consistent with the second dielectric transition and can be ascribed to structure phase transition. The conductivity reached $9.11 \times 10^{-4} \text{ S cm}^{-1}$ at 403 K. The conductivity of 1 in the temperature region of 333–368 K and 373–403 K was fitted by the Arrhenius expression as follows:

$$\ln(\delta) = \ln(\delta_0) - \frac{E_a}{kT},$$

where σ_0 = preexponential factor, E_a = activation energy, and k = Boltzmann's constant. The fitted activation energy is 0.84 eV in the temperature region of 333–368 K and 0.73 eV in the temperature region of 373–403 K.

The complex-plane impedance plots of 2 at the selected temperature are shown in Figure 7C and Supplementary Figure S6. Similar to Figure 7A, a large semicircle and an inclined spike occurred at high-frequency and low-frequency regions, respectively. The thermally activated conduction mechanism is also observed for 2. The temperature dependent conductivity is plotted in the form of $\ln\sigma_{dc}$ versus $1,000/T$ (Figure 7D). From 363 to 368 K, the conductivity of 2 steeply increases (similar to the dielectric data), and the σ value is $1.29 \times 10^{-6} \text{ S cm}^{-1}$ at 363 K and $1.38 \times 10^{-5} \text{ S cm}^{-1}$ at 368 K. The Arrhenius equation is used to fit the conductivity of 2, and the activation energy is 0.65 eV in the temperature region of 333–363 K and 0.70 eV in the temperature region of 373–388 K.

Although switchable magnetic state transition has usually been reported in nickel dithiolene complexes, the investigation mainly concerns the relationship between magnetic and structure phase transition. To date, the dielectric state transition with the thermal hysteresis loop in metal-dithiolene complexes is very rare. To the best of our knowledge, 2 is the first example of metal-dithiolene complexes in both aspects of exhibiting magnetic



transitions and dielectric transition with the thermal hysteresis loop.

Conclusion

In summary, two low-dimensional $S = \frac{1}{2}$ spin compounds, assembled from the paramagnetic $[\text{Ni}(\text{mnt})_2]^-$ anions with the methylimidazolium cation, show excellent dielectric switchable properties with the thermal hysteresis loop. Two-step dielectric state transition of 1 can be attributed to the reorientation of the polar cations and crystal to mesophase transition, which is consistent with the DSC results. Dielectric phase transition at high temperature of two compounds is associated with the conductivity anomaly. The conductivity of mesophase for 1 and 2 is higher than that of the corresponding crystal phase. Another striking feature is that the high-temperature magnetic transition has a non-common hysteresis loop for

2 and is accompanied with the crystal–mesophase transition. This study opens up new avenues to the design and preparation of multi-functional bistability material systems combining magnetic, dielectric, and conductivity properties.

Data availability statement

The original contributions presented in the study are included in the article/[Supplementary Materials](#); further inquiries can be directed to the corresponding author.

Author contributions

HD conceived the idea for this study, designed the experiments, and revised the manuscript. SY and HZ performed the experiments, analyzed the data, and wrote the

manuscript. WX and HZ assisted with sample characterization and provided some suggestions.

Acknowledgments

The authors thank the Natural Science Foundation of Jiangsu Province for the financial support (grant no.: BK20171125).

Conflict of interest

The authors declare that the research was conducted in the absence of any commercial or financial relationships that could be construed as a potential conflict of interest.

References

- Akutagawa, T., Koshinaka, H., Sato, D., Takeda, S., Noro, S. I., Takahashi, H., et al. (2009). Ferroelectricity and polarity control in solid-state flip-flop supramolecular rotators. *Nat. Mat.* 8, 342–347. doi:10.1038/nmat2377
- Asghar, M. A., Zhang, S., Khan, T., Sun, Z., Zeb, A., Ji, C., et al. (2016). Reversible phase transition driven by order-disorder transformations of metal-halide moieties in $[(C_6H_{14})NH_2]_2CuBr_4$. *J. Mat. Chem. C* 4, 7537–7540. doi:10.1039/c6tc02034h
- Barsoukov, E., and Macdonald, J. R. (2018). *Impedance spectroscopy theory, experiment, and applications*. Dallas, TX; Chapel Hill, NC: John Wiley & Sons.
- Champagne, B., Plaquet, A., Pozzo, J. L., Rodriguez, V., and Castet, F. (2012). Nonlinear optical molecular switches as selective cation sensors. *J. Am. Chem. Soc.* 134, 8101–8103. doi:10.1021/ja302395f
- CrysAlis (2004). *CrysAlis V1.171*. Poland: Oxford Diffraction Ltd.
- Davison, A., and Holm, H. R. (1967). *Inorg. Synth.* Cambridge: Mass 10, 8.
- Delaire, J. A., and Nakatani, K. (2000). Linear and nonlinear optical properties of photochromic molecules and materials. *Chem. Rev.* 100, 1817–1846. doi:10.1021/cr980078m
- Duan, H. B., Chen, X. R., Yang, H., Ren, X. M., Xuan, F., and Zhou, S. M. (2013). Disorder-order transformation and significant dislocation motion cooperating with a surprisingly large hysteretic magnetic transition in a nickel-bisdithiolene spin system. *Inorg. Chem.* 52, 3870–3877. doi:10.1021/ic302571p
- Duan, H. B., Ren, X. M., Shen, L. J., Jin, W. Q., Meng, Q. J., Tian, Z. F., et al. (2011). A low-dimensional molecular spin system with two steps of magnetic transitions and liquid crystal property. *Dalton Trans.* 40, 3622. doi:10.1039/c0dt01704c
- Fu, D. W., Cai, H. L., Liu, Y., Ye, Q., Zhang, W., Zhang, Y., et al. (2013). Diisopropylammonium bromide is a high-temperature molecular ferroelectric crystal. *Science* 339, 425–428. doi:10.1126/science.1229675
- Hamaguchi, H., and Ozawa, R. (2005). Structure of ionic liquids and ionic liquid compounds: Are ionic liquids genuine liquids in the conventional sense? *Adv. Chem. Phys.* 131, 85. doi:10.1002/0471739464.ch3
- Hang, T., Zhang, W., Ye, H. Y., and Xiong, R. G. (2011). Metal-organic complex ferroelectrics. *Chem. Soc. Rev.* 40, 3577. doi:10.1039/c0cs00226g
- Jiang, X., Duan, H. B., Jellen, M. J., Chen, Y., Chung, T. S., Liang, Y., et al. (2019). Thermally activated transient dipoles and rotational dynamics of hydrogen-bonded and charge-transferred diazabicyclo [2.2.2]octane molecular rotors. *J. Am. Chem. Soc.* 141, 16802–16809. doi:10.1021/jacs.9b07518
- Lochenie, C., Bauer, W., Railliet, A. P., Schlamp, S., Garcia, Y., and Weber, B. (2014). Large thermal hysteresis for iron(II) spin crossover complexes with *N*-(Pyrid-4-yl)isonicotinamide. *Inorg. Chem.* 53, 11563–11572. doi:10.1021/ic501624b
- Mariappan, C. R., Govindaraj, G., and Roling, B. (2005). Lithium and potassium ion conduction in A3TiB/P3O12 (A=Li, K; B'=Zn, Cd) NASICON-type glasses. *Solid State Ionics* 176, 723–729. doi:10.1016/j.ssi.2004.11.008
- Matsumoto, T., Newton, G. N., Shiga, T., Hayami, S., Matsui, Y., Okamoto, H., et al. (2014). Programmable spin-state switching in a mixed-valence spin-crossover iron grid. *Nat. Commun.* 5, 3865. doi:10.1038/ncomms4865

Publisher's note

All claims expressed in this article are solely those of the authors and do not necessarily represent those of their affiliated organizations, or those of the publisher, the editors, and the reviewers. Any product that may be evaluated in this article, or claim that may be made by its manufacturer, is not guaranteed or endorsed by the publisher.

Supplementary material

The Supplementary Material for this article can be found online at: <https://www.frontiersin.org/articles/10.3389/femat.2022.977164/full#supplementary-material>

Salinga, M., and Wuttig, M. (2011). Phase-change memories on a diet. *Science* 332, 543–544. doi:10.1126/science.1204093

Samoc, M., Gauthier, N., Cifuentes, M. P., Paul, F., Lapinte, C., and Humphrey, M. G. (2006). Electrochemical switching of the cubic nonlinear optical properties of an arylidethynyl-linked heterobimetallic complex between three distinct states. *Angew. Chem. Int. Ed.* 45, 7376–7379. doi:10.1002/anie.200602684

Seredyuk, M., Gaspar, A. B., Ksenofontov, V., Galyametdinov, Y., Kusz, J., and Gütlich, P. (2008). Iron(II) metallomesogens exhibiting coupled spin state and liquid crystal phase transitions near room temperature. *Adv. Funct. Mat.* 18, 2089–2101. doi:10.1002/adfm.200800049

Sheldrick, G. M. (1997). *SHELXL-97, program for crystal StructureRefinement*. Göttingen, Germany: Göttingen University.

Stuart, M. A. C., Huck, W. T. S., Genzer, J., Mller, M., Ober, C., Stamm, M., et al. (2010). Emerging applications of stimuli-responsive polymer materials. *Nat. Mat.* 9, 101–113. doi:10.1038/nmat2614

Su, S. Q., Kamachi, T., Yao, Z. S., Huang, Y. G., Shiota, Y., Yoshizawa, K., et al. (2015). Assembling an alkyl rotor to access abrupt and reversible crystalline deformation of a cobalt(II) complex. *Nat. Commun.* 6, 8810. doi:10.1038/ncomms9810

Sun, Z., Luo, J., Chen, T., Li, L., Xiong, R. G., Tong, M. L., et al. (2012). Distinct molecular motions in a switchable chromophore dielectric 4-*N,N*-Dimethylamino-4'-*N'*-methylstilbazolium trifluoromethanesulfonate. *Adv. Funct. Mat.* 22, 4855–4861. doi:10.1002/adfm.201201770

Sun, Z., Zhang, S., Ji, C., Chen, T., and Luo, J. (2014). Exceptional dielectric performance induced by the stepwise reversible phase transitions of an organic crystal: Betainium chlorodifluoroacetate. *J. Mat. Chem. C* 2, 10337–10342. doi:10.1039/c4tc01925c

Tian, Z. F., Duan, H. B., Ren, X. M., Lu, C. S., Li, Y. Z., Song, Y., et al. (2009). Two spin-peierls-like compounds exhibiting divergent structural features, lattice compression, and expansion in the low-temperature phase. *J. Phys. Chem. B* 113, 8278–8283. doi:10.1021/jp8100333

Weber, B. (2009). Spin crossover complexes with N4O2 coordination sphere—the influence of covalent linkers on cooperative interactions. *Coord. Chem. Rev.* 253, 2432–2449. doi:10.1016/j.ccr.2008.10.002

Weber, B., Bauer, W., and Obel, J. (2008). An iron(II) spin-crossover complex with a 70 K wide thermal hysteresis loop. *Angew. Chem. Int. Ed.* 47, 10098–10101. doi:10.1002/anie.200802806

Xu, G. C., Ma, X. M., Zhang, L., Wang, Z. M., and Gao, S. (2010). Disorder-Order ferroelectric transition in the metal formate framework of $[NH_4][Zn(HCOO)_3]$. *J. Am. Chem. Soc.* 132, 9588–9590. doi:10.1021/ja104263m

Yu, S. S., Duan, H. B., Chen, X. R., Tian, Z. F., and Ren, X. M. (2013). Observation of intramolecular vibrations cooperating with the magnetic phase transition in a nickel-bis-dithiolene compound. *Dalton Trans.* 42, 3827. doi:10.1039/c2dt31519j

Yu, Y., Nakano, M., and Ikeda, T. (2003). Directed bending of a polymer film by light. *Nature* 425, 145. doi:10.1038/425145a